Preprints of the 21st IFAC World Congress (Virtual)
Berlin, Germany, July 12-17, 2020

Eco-Driving for Energy Efficient Cornering of Electric Vehicles in Urban Scenarios ⋆

G.P. Padilla C. Pelosi C.J.J. Beckers M.C.F. Donkers

Eindhoven University of Technology, Netherlands
(e-mail: {g.p.padilla.cazar,c.j.j.beckers,m.c.f.donkers}@tue.nl, c.pelosi@student.tue.nl)

Abstract: In this paper, we propose a model for eco-driving that considers cornering effects. The proposed model purely relies on the geometric configuration of the vehicle and road. Consequently, we propose an eco-driving optimal control problem formulation that is suitable for both straight and curved trajectories in urban scenarios. Moreover, it can be applied for vehicles with front wheel drive (FWD) or rear wheel drive (RWD). We use a case study for an electric vehicle executing cornering maneuvers to validate the proposed approach with a high fidelity vehicle model. Results show an approximated improvement of 8% in energy savings with respect to traditional eco-driving strategies, especially in trajectories with large curvatures.

Keywords: Energy management system, optimal control, velocity control, electric vehicles, vehicle dynamics.

1. INTRODUCTION

In recent years, electrification of transport systems, or electromobility (Grauers et al., 2013), has been raised as a promising approach to mitigate environmental effects caused by CO_2 emissions and to face the imminent depletion of fossil fuels reserves. However, the goal of complete acceptance of electromobility in the market is still far and several problems like range anxiety still have to be solved. Range anxiety is defined as the fear experienced by drivers of having insufficient energy to arrive to the next charging station (AccessScience Editors, 2014). In general, energy management strategies are a direct method to reduce range anxiety. In particular, the capability to extend driving range by reducing power demand demonstrated by eco-driving techniques has positioned these approaches as strong tools alleviate effects of range anxiety, e.g., Flores et al. (2019).

As a general concept, eco-driving is a selection of energy efficient driving strategies (Bingham et al., 2012), which can be obtained by solving an optimal control problem (OCP) that aims to find optimized velocity profiles that reduce the total consumption of the vehicle, e.g., see Sciarretta et al. (2015). This concept has been studied in terms of the energy source of the vehicle, e.g., for conventional vehicles in Maamria et al. (2017), for hybrid electric vehicles by Khalik et al. (2018), and for electric vehicles by Petit and Sciarretta (2011). Eco-driving has also been analysed in terms of the surrounding operational conditions. For urban scenario cases, Nunzio et al. (2013) have included traffic light information into the eco-driving formulation, Henriksson et al. (2017) use traffic statistic data to create velocity corridors where solutions the eco-driving OCP lay, and Han et al. (2018) consider the effects of the preceding vehicle in the problem formulation. Interestingly, the literature about eco-driving for urban trajectories where cornering is considered is scarce.

In Beckers et al. (2020), a high-fidelity model is presented to calculate additional energy losses in the tires during cornering of the vehicle. The results presented in this work have shown that energy losses during cornering maneuvers should not be neglected. Cornering losses become relevant during urban scenarios where the vehicle might follow routes where several turning maneuvers are performed. Often, eco-driving formulations that consider the road curvature include a constraint linked to the centripetal acceleration, which indirectly limits the maximum velocity during cornering, e.g., Polterauer et al. (2019). In this case, the cornering losses are not directly considered in the formulation. As a result, the solutions obtained are unlikely to be energy optimal during the cornering maneuver. An interesting case is presented in Ikezawa et al. (2017), where a dynamical vehicle model is used to describe a simplified model that can be used to formulate an eco-driving OCP. Unfortunately, this description depends on cornering stiffness of the tires, which can show significant variations between vehicles and tire conditions. Other approaches aim to achieve energy efficient cornering by applying energy efficient torque vectoring to the vehicle (Edrén et al., 2019). Unfortunately, these approaches partially neglect the eco-driving concept by only focusing on the cornering maneuver itself.

In this paper, we aim to bridge the gap observed in literature by extending the current eco-driving OCP formulation of Padilla et al. (2018) to consider cornering effects. In particular, our main contributions are the use of a kinematic bicycle model to approximate the dissipative forces produced during cornering in the longitudinal direction of the vehicle. This model purely depends on the geometry of the road and the vehicle, which makes it suitable to be deployed in real applications where the tire properties are often unknown. Thus, we propose a trajectory dependent model for eco-driving that can be used for vehicles with front wheel drive (FWD) and rear wheel drive (RWD). This allow us to formulate generalized eco-driving OCP that is suitable to be used in urban routes.

⋆ This work has received financial support from the Horizon 2020 program of the European Union under the grant 'Electric Vehicle Enhanced Range, Lifetime And Safety Through INGenious battery management' (EVERLASTING-713771).

2. A TRAJECTORY-DEPENDENT MODEL FOR ECO-DRIVING

In this section, we provide a general vehicle dynamical model to be used in the eco-driving optimal control problem proposed in this paper. To this end, we analyse the representations used for straight trajectories, which coincides with traditional models used for eco-driving in the current literature. Later, we propose a generalized description of the dissipative forces for curved trajectories, which are often present in urban scenarios. Finally, we show that the generalized models obtained for curved trajectories can easily describe the dynamics for straight trajectories as well.

The main objective of eco-driving strategies is to obtain energy optimal velocity profiles. In general, the dynamical models considered in traditional eco-driving approaches represent the longitudinal vehicle dynamics by the interaction between the traction force in the longitudinal axis $F_l(t)$ and dissipative forces $F_d(t)$, i.e.,

$$ma = F_l - F_d, \tag{1}$$

where m represents the equivalent mass of the vehicle, and $a(t) = \frac{\mathrm{d}v}{\mathrm{d}t}$ is the vehicle acceleration. The definition of $F_d(t)$ in (1) can vary depending on the trajectory that the vehicle is describing. Specifically, we consider the cases for straight and curved trajectories below.

2.1 Straight Trajectories

A traditional assumption for eco-driving problem formulations is that the vehicle moves along a straight trajectory such that the dissipative force is given by

$$F_d(v,s) = \underbrace{\sigma_d v^2}_{F_{air}} + \underbrace{mg(c_r\cos(\alpha(s)) + \sin(\alpha(s)))}_{F_{roll+grav}}, \tag{2}$$

where $v(t)$ represents the vehicle velocity, $s(t)$ describes displacement, $\alpha(s(t))$ is the road grade, g is the gravitational acceleration, $c_r > 0$ is the rolling resistance coefficient, and $\sigma_d = \frac{1}{2}c_d\rho_a A_f$ with the aerodynamical drag coefficient $c_d > 0$, air density ρ_a and frontal area of the vehicle A_f. In the right-hand side of (2), the term F_{air} represents the force produced by aerodynamical drag, and the term $F_{roll+grav}$ is the force connected to rolling resistance and gravity. These forces are depicted in Fig. 1 for a straight trajectory case. Finally, by defining the total traction force provided by the electric motor $F_u(t)$, we see that

$$F_l = F_u \tag{3}$$

Note that this relationship is independent of the drive configuration of the vehicle, i.e., (3) holds for both RWD and FWD configurations.

The assumption of a straight trajectory is widely adopted in literature, see, e.g., Sciarretta et al. (2015) and the references therein. It is intuitive to validate this assumption for vehicles driving in highways, where trajectories with large curvature are not often present. However, cornering actions are often needed during a typical urban trajectory. Moreover, the curvatures of these trajectories are significantly higher than in highways, which is translated into a larger energy consumption that should not be neglected, e.g., (Beckers et al., 2020; Ikezawa et al., 2017).

2.2 Curved Trajectories

The main contribution of this section is the inclusion of cornering effects in the model used for eco-driving OCP

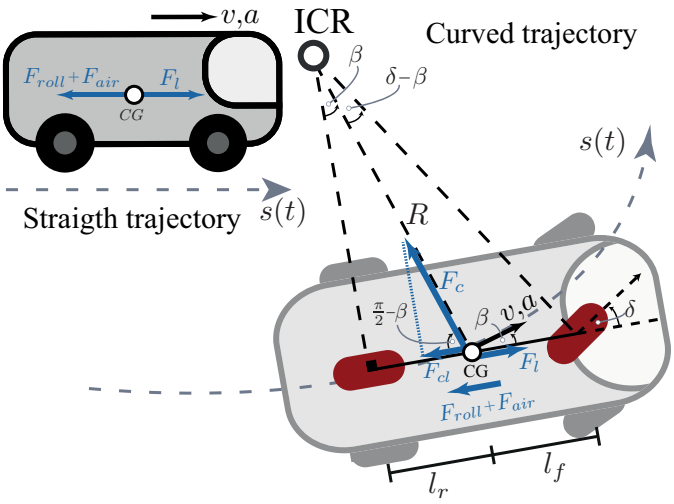

Fig. 1. Forces on the londitudinal axis for both straight and curved trajectories.

in urban scenarios, i.e., assuming curved trajectories. The effect of cornering in terms of energy consumption has been discussed in Beckers et al. (2020), where a detailed nonlinear model has been developed and validated experimentally. This model describes additional tire slip losses during cornering. The results presented in the aforementioned work show that the energy consumed as consequence of cornering can be significant. In this section, we follow a simplified approach to approximate the effects of cornering into a low-complexity model that will be used to formulate the eco-driving OCP in Section 3.

Let us consider the curved trajectory observed in Fig. 1, which is characterized by a position-dependent curvature function $K(s)$, where the curvature is defined as the reciprocal of the radius $R(s)$, i.e.,

$$K(s) = \tfrac{1}{R(s)}. \tag{4}$$

The radius R is measured from the instantaneous center of rotation (ICR) to the vehicle center of gravity (CG). We assume that the CG shown in Fig. 1 is located at a distance l_r from the rear wheel axle and a distance l_f form the front wheel axle. Moreover, the vehicle depicted in Fig. 1 has a front wheel steering angle $\delta(s) \in [-\frac{\pi}{2}, \frac{\pi}{2}]$.

In order to analyse the interaction of traction and dissipative forces in this case, we use a kinematic bicycle model. Despite the simplicity of a kinematic bicycle model, it can achieve similar results as a dynamical bicycle model for vehicle control purposes (Kong et al., 2015). The bicycle model considers that the two front and rear wheels are respectively lumped into one single front and rear wheel, which in Fig. 1 are represented in red color. Even thought the kinematic version of this model is strictly true only for low lateral vehicle accelerations, applying this model to high-velocity corners will result is an over-estimate of the cornering energy, thereby making the model quantitatively conservative. Moreover, we assume vehicles with front-wheels-only steering systems, implying that the rear wheel will be aligned with the longitudinal axis of the vehicle for the entire route. For the sake of simplicity, we assume that the dissipative forces F_{roll} and F_{air} are aligned with the longitudinal axis of the vehicle. Note that the velocity of the vehicle $v(t)$ is tangential to the trajectory and shows an angle $\beta(s(t)) \in [-\frac{\pi}{2}, \frac{\pi}{2}]$ with respect to the longitudinal axis, which is given by

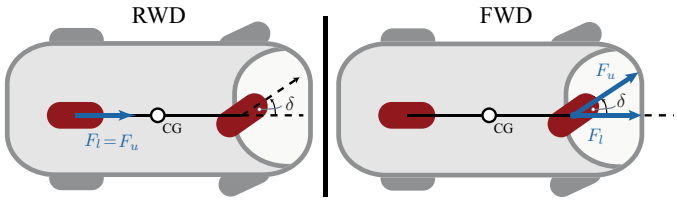

Fig. 2. Traction force for RWD and FWD configurations.

$$\beta(s) = \arcsin\left(l_r K(s)\right) \tag{5}$$

The total centripetal force applied at CG and its projection into the longitudinal vehicle axis are given by

$$F_c(v,s) = mv^2K(s), \tag{6}$$

and

$$F_{cl}(v,s) = F_c(v,s)\cos(\tfrac{\pi}{2} - \beta(s(t))) = ml_r v^2 K(s)^2, \tag{7}$$

respectively.

An analysis of the forces acting on the longitudinal axis of the vehicle shows that for curved trajectories the total dissipative force in that direction is given by

$$F_d(v,s) = F_{roll+grav} + F_{air} + F_{cl}. \tag{8}$$

Note that projection of the centripetal force into the longitudinal axis (7) can be physically interpreted as a lumped approximation in the longitudinal direction of the lateral forces generated on the tires during cornering. From (2) and (7), it is possible to rewrite (8) as

$$F_d(v,s) = mg(c_r\cos(\alpha(s)) + \sin(\alpha(s))) + (\sigma_d + ml_r K(s)^2)v^2. \tag{9}$$

Unlike to the approach of Ikezawa et al. (2017), the dissipating force introduced by cornering F_{cl} is an approximation that only depends on the geometric configuration of the vehicle and the road, which comes as a consequence of the use of a kinematic model. In Section 4, we will use a numerical example to show that albeit the simplicity of the obtained approximation, it properly captures the behavior of the vehicle during cornering for control purposes.

The traction force in the longitudinal direction F_l depends on the drive configuration of the vehicle, i.e., in a RWD configuration the total motor traction force $F_u(t)$ is directly applied directly to the longitudinal direction of the vehicle, while for FWD case only a fraction of $F_u(t)$ is applied in the longitudinal direction. This idea is depicted in Fig. 2, where the traction forces for the two drive configurations are shown. It is clear to see that the traction force for a vehicle with RWD can be described by (3). On the other had, the traction force in the longitudinal direction for a FWD vehicle depends on the steering angle as

$$F_l(F_u, s) = F_u\cos(\delta(s)), \tag{10}$$

where according to the kinematic bicycle model

$$\delta(s) = \arctan\left(\frac{l_f + l_r}{l_r}\tan\left(\beta(s)\right)\right). \tag{11}$$

After substituting (5) into (11) and applying a composition of trigonometric and inverse trigonometric functions, the traction force into the longitudinal direction (12) can be reformulated as

$$F_l(F_u, s) = \frac{F_u}{\sqrt{1 + \frac{(l_f + l_r)^2 K^2(s)}{1 - l_r^2 K^2(s)}}}. \tag{12}$$

The projection of the centripetal force and the traction force in the direction of motion allows us to generalize the longitudinal vehicle dynamics (1) model for curved trajectories as

$$ma = F_l(F_u, s) - F_d(v, s), \tag{13}$$

where $a(t) = \frac{\mathrm{d}v}{\mathrm{d}t}$ is the acceleration in the tangential direction to the trajectory. Considering that the forces are analyzed in the longitudinal axis of the vehicle, the use of $a(t)$ instead of the longitudinal acceleration $a_l(t)$ in (13) is justified by a small angle approximation such that $a_l(t) = a(t)\cos(\beta(s)) \approx a(t)$. Additionally in (13), $F_d(v,s)$ is given by (9), and $F_l(F_u, s)$ is described by (3) and (12) for vehicles with FWD and RWD, respectively. As a final observation, it should be noted that taking $K(s) = 0$ implies that the vehicle moves on a straight trajectory. For this specific case, (9) is equivalent to (2), which represent the dissipating forces for a straight trajectory. Similarly, for FWD vehicles (12) is equivalent to (3), which describes the traction force in the longitudinal direction for vehicles driving in straight trajectories. These observations show the generality of the proposed models.

3. OPTIMAL CONTROL PROBLEM

A continuous-time optimal control problem (OCP) formulation that represents the eco-driving problem for urban city scenarios is provided in this section. In particular, we will extend the eco-driving formulation proposed in Padilla et al. (2018) to include the cornering effects captured by the trajectory dependent models presented in the previous section. Additionally, we discuss the differences between the OCP proposed in this paper and common approaches of eco-driving for cornering available in literature.

3.1 Problem Formulation

For a route with given curvature $K(s)$ and road grade $\alpha(s)$, eco-driving aims to minimize the aggregative power $P(v(t), F_u(t))$ over a fixed period of time $[t_\mathrm{o}, t_\mathrm{f}]$ required by a vehicle driving a trajectory $s(t) \in [s_\mathrm{o}, s_\mathrm{f}]$, while being subject to position dependent velocity and acceleration bounds $v(t) \in [\underline{v}(s), \overline{v}(s)]$, $a(t) \in [\underline{a}(s), \overline{a}(s)]$, respectively. Moreover, the vehicle longitudinal dynamics and initial final conditions for position and velocity are considered. A mathematical formulation of the eco-driving problem as an OCP is given by

$$\min_{s(t),v(t),a(t),F_u(t)} \int_{t_o}^{t_f} P(v(t), F_u(t))\mathrm{d}t \tag{14a}$$

$$\text{subject to} \quad ma(t) = F_l(F_u(t), s(t)) - F_d(v(t), s(t)), \tag{14b}$$

$$\tfrac{\mathrm{d}}{\mathrm{d}t}s(t) = v(t), \tag{14c}$$

$$\tfrac{\mathrm{d}}{\mathrm{d}t}v(t) = a(t), \tag{14d}$$

$$s(t_\mathrm{o}) = s_\mathrm{o}, \quad s(t_\mathrm{f}) = s_\mathrm{f} \tag{14e}$$

$$v(t_\mathrm{o}) = v_\mathrm{o}, \quad v(t_\mathrm{f}) = v_\mathrm{f} \tag{14f}$$

$$a(t)^2 + v(t)^4 K(s(t))^2 \leq (\mu_s g)^2, \tag{14g}$$

$$\underline{v}(s(t)) \leq v(t) \leq \overline{v}(s(t)), \tag{14h}$$

$$\underline{a}(s(t)) \leq a(t) \leq \overline{a}(s(t)), \tag{14i}$$

where the power consumed by the electric motor and driveline at a given time instant is

$$P(v, F_u) = \beta_2 F_u^2 + \beta_1 v F_u + \beta_0 v^2 \tag{15}$$

with positive coefficients β_2 to penalize the Ohmic losses, β_1 to describe effective power consumed, and β_0 that penalizes the friction losses in the electric motor. Note that the power consumption (15) considers regenerative braking. The longitudinal vehicle dynamics are described by

(14b) with the definitions provided for (13), the time evolution of acceleration, velocity and position are described by (14d) and (14c), and boundaries for position of velocity are represented by (14e) and (14f), respectively. Finally, (14g) represents a constraint imposed on the total acceleration of the vehicle, where $\mu_s > 0$ is a friction coefficient dependent on the characteristics of the tires and the road conditions. In order to give a physical justification to (14g), let us note that the maximum friction force between the road and tires is given by $F_{fric} = m\mu_s g$. For safety reasons, is required to avoid the vehicle to slip, which implies that the total force applied to the vehicle is lower than the maximum friction force during normal operation, i.e.,

$$(ma(t))^2 + (mv(t)^2 K(s(t)))^2 \leq (m\mu_s g)^2, \qquad (16)$$

which can be simplified into (14g). The first term in the left hand side of (16) represents the resultant force applied to the vehicle in the tangential direction of the trajectory, and the second term is the centripetal force. Note that (14g) is mainly relevant during cornering. During straight trajectories this constraint is inactive because upper acceleration bound in (14i) is expected to satisfy $\overline{a}(s) \leq \mu_s g$.

3.2 Effects of Cornering

From the scarce literature about eco-driving approaches that consider cornering effects, it is possible to note that often the OCP formulation includes a constraint linked to the centripetal acceleration of the vehicle, see, e.g., Polterauer et al. (2019), which is similar to (14g). This type of hard constraint implicitly imposes a limit to the maximum velocity during cornering. In the approach presented in this paper, we improve the representation of cornering effects by including those effects in longitudinal vehicle dynamics, i.e., (14b). This specific modeling choice can be seen as a soft constraint that highly penalizes the velocity while cornering. To this end, we will use a simplified example that, without losing generality, allows us to observe the effects of cornering in the OCP (14).

Let us consider a RWD vehicle, driving in a circular trajectory on a flat road, i.e., $K(s) = \frac{1}{R}$ and $\alpha(s) = 0$. It is possible to find an equivalent formulation fo the OCP (14) by substituting (14b) into (14a) (see , e.g., (Boyd and Vandenberghe, 2004, §4.1.3)), leading to

$$\min_{s(t),v(t),a(t)} \quad \int_{t_o}^{t_f} P(v(t), ma(t) + F_d(v(t), s(t)))\mathrm{d}t \qquad (17)$$
$$\text{subject to} \quad \text{(14c)-(14i)},$$

in which

$$P(v, ma+F_d(v,s)) = \beta_2\big(m(a+gc_r)+(\sigma_d+ml_rK^2)v^2\big)^2 + \beta_1 v\big(m(a+gc_r)+(\sigma_d+ml_rK^2)v^2\big)+\beta_0 v^2. \qquad (18)$$

Thus, we can note the the term ml_rK^2 drastically penalizes velocity in the new cost function. This penalization, depends quadratically on the road curvature, which implies that the optimal solution might show lower decelerations during cornering maneuvers.

4. CASE STUDY

In this section, we study an electric vehicle executing a cornering maneuver in an urban environment with different curvatures. The advantages of the model and OPC formulation presented in this paper are highlighted in this example. To this end, we will contrast the results with traditional eco-driving approaches. Moreover, we will show the relevance of the proposed approach using an experimentally validated high-fidelity model to calculate the instantaneous power and total energy consumption produced during the cornering maneuvers analyzed.

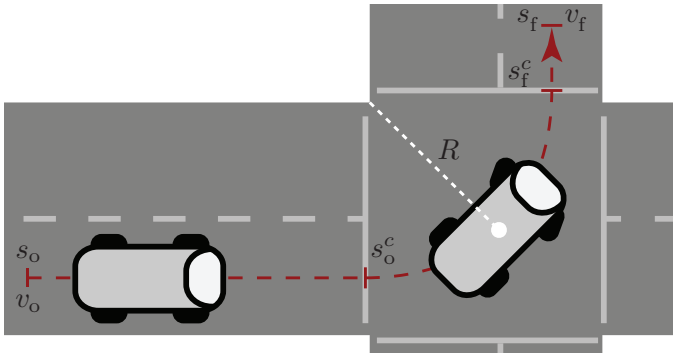

Fig. 3. Urban intersection considered in the case study.

Let us consider an electric vehicle with RWD and parameters listed in Table 1. The vehicle executes a cornering maneuver on a city intersection as is depicted in Fig. 3, which curvature is defined as

$$K(s) = \begin{cases} \dfrac{1}{R} & \text{for } s_o^c \leq s \leq s_f^c, \\ 0 & \text{otherwise;} \end{cases} \qquad (19)$$

where s_o^c is the position where the corner begins and s_f^c is the final corner position. The curvature (19), will be specified for three different scenarios that are detailed in Table 2.

The OCP (14) is formulated using the parameters in Table 1. To find the solutions of this OCP, we dicretize the problem (14) and solve a static optimization problem. It is important to remark that this paper focuses on the modeling and OPC formulation rather than in the methodology to find the solution. However, the interested reader can follow the methodology detailed in Padilla et al. (2018) and Flores et al. (2019). The optimal solutions to (14) are depicted in Fig. 4 as velocity and acceleration profiles for each scenario considered in the case study. Note that the vertical lines depicted in both profiles indicate the initial and final positions of the curved section of the trajectory. It can be observed that the vehicle decelerates before entering the curved section of the trajectory. When the vehicle enters the curved section of the trajectory the deceleration rate is reduced and approximately at halfway along the curved section the vehicle begins accelerating. As soon as the vehicle leaves the curved section of the trajectory the acceleration is immediately increased. Interestingly, the differences between scenarios considered is clearly observed in the velocity profiles, where at higher curvatures lower velocities are observed in the curved section of the trajectory. This result is expected because velocity is highly penalized for high curvatures in the road. This effect has been discussed in Section 3.2.

Table 1. Vehicle and OCP parameters

Par.	Value	Units	Par.	Value	Units
m	15000	$[kg]$	σ_d	3.24625	$[Ns^2/m^2]$
c_r	0.007	–	μ_s	0.35	–
β_0	0.292	$[ws^2/m^2]$	β_1	1.005	–
β_2	2.652e-4	$[w/N^2]$	s_0	0	$[m]$
s_f	150	$[m]$	v_0	30	$[m/s]$
v_f	35	$[m/s]$	$\overline{v}$	60	$[m/s]$
$\underline{v}$	0	$[m/s]$	$\overline{a}$	0.2g	$[m/s^2]$
$\underline{a}$	-0.2g	$[m/s^2]$			

In order to highlight the advantages of our general approach, we compare the optimal solution to the OCP (14) with a traditional eco-driving OCP formulation. Specifically, a traditional OCP considers the constraint (14g), but the cornering effects in (14b) are neglected. In Fig. 5, the optimal velocity and acceleration profiles for traditional and general eco-driving formulations are presented for the specific scenario where $R = 14\,[m]$. Note that the velocity profile of the traditional approach shows constant velocity during the curved section of the road, which also indicates zero acceleration during that section. This is expected since traditional eco-driving strategies avoids changes in acceleration to reduce energy consumption. As a consequence, the vehicle crosses the curved section with the maximum possible velocity, which is defined by constrain (14g). On the other hand, the optimal strategy obtained by the general approach proposed in this paper shows lower velocities during the curved section, which is connected to the velocity being penalized by the curvature of the road. This causes non-zero longitudinal acceleration in the curved section. The effects of both strategies in terms of power consumption can be observed in in Fig. 6, where the instantaneous cumulative power consumption produced by these two strategies is depicted. Here, we use the experimentally validated high-fidelity model from Beckers et al. (2020) to calculate the cornering losses, in combination with instantaneous power consumed by the inertia, aerodynamical drag, rolling resistance, and electric machine losses. As expected, the main difference between both strategies are observed in the curved section of the trajectory. For the traditional strategy, the power

Table 2. Parameters for different scenarios.

R	s_o^c	s_f^c
12 $[m]$	70 $[m]$	$70+R\pi/2$ $[m]$
14 $[m]$	70 $[m]$	$70+R\pi/2$ $[m]$
17 $[m]$	70 $[m]$	$70+R\pi/2$ $[m]$

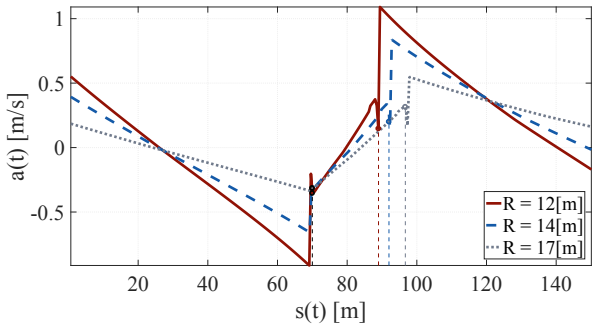

(a) Acceleration profiles.

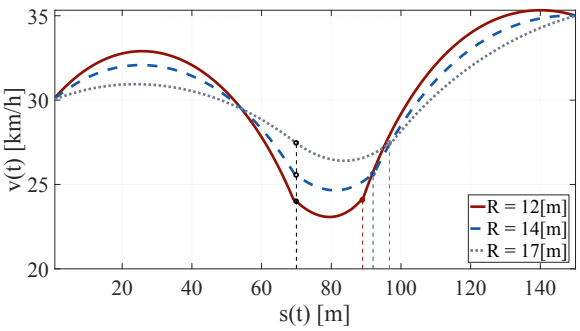

(b) Velocity profiles.

Fig. 4. Optimal solutions to the OCP (14) for different curvatures.

Table 3. Comparison of energy consumption between strategies.

Scenario	**Tot. Energy (Traditional)**	**Tot. Energy (General)**	**Diff. %**
$R = 12\,[m]$	820.2 $[kJ]$	757.6 $[kJ]$	8.26
$R = 14\,[m]$	687.5 $[kJ]$	658.2 $[kJ]$	4.45
$R = 17\,[m]$	574.2 $[kJ]$	573.4 $[kJ]$	0.14

losses due to cornering and electric machine losses are constant during the curved section, while the general strategy indicates virtually no electric machine losses during the first half of the curved trajectory. This shows that the cornering maneuver obtained form the general strategy is more energy efficient than the traditional counterpart. This observation is reinforced by simulations performed on the rest of the scenarios considered in this case study.

In Fig. 7, we present the cumulative energy obtained by using the traditional and general strategies for scenarios with three different curvatures, and in Table 3, we summarize the total energy calculated with the high-fidelity model for each case and strategy. The trend observed from these results indicates that the general strategy proposed in this paper is able to improve the energy efficiency of the vehicle for all the considered scenarios. In fact, the proposed eco-driving strategy saves a larger amount of energy for scenarios with larger curvatures, while for roads with small curvature the total consumption of the general strategy tends to approximate to the traditional approach. This is a consistent result since our OCP formulation resembles traditional eco-driving formulations when roads with no curvature are considered, as has been discussed in Section 2.2. Remarkably, in Fig. 7, it is possible to see that a higher energy efficiency of the proposed strategy mainly comes from a reduction of the energy losses in the electric machine.

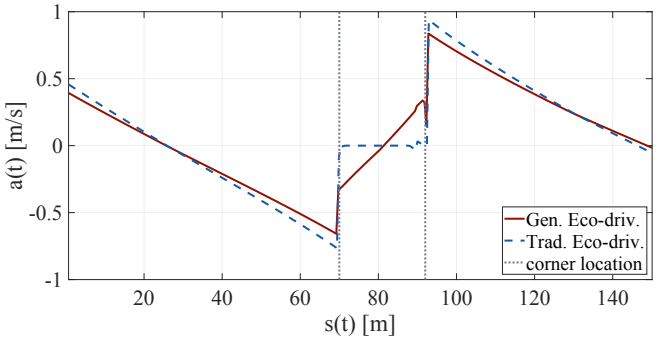

(a) Acceleration profiles.

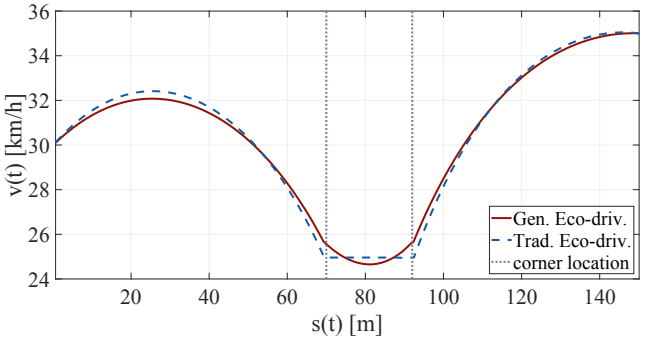

(b) Velocity profiles.

Fig. 5. Comparison for OCP formulations for cornering scenario with $R = 14\,[m]$.

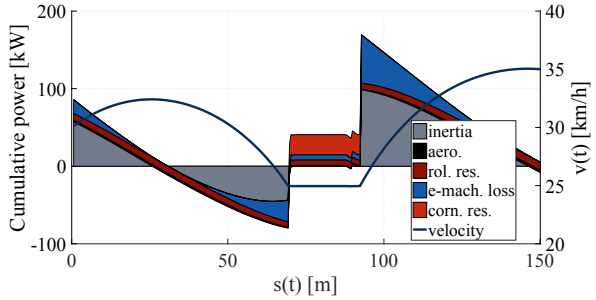

(a) Tradditional eco-driving aprpoach.

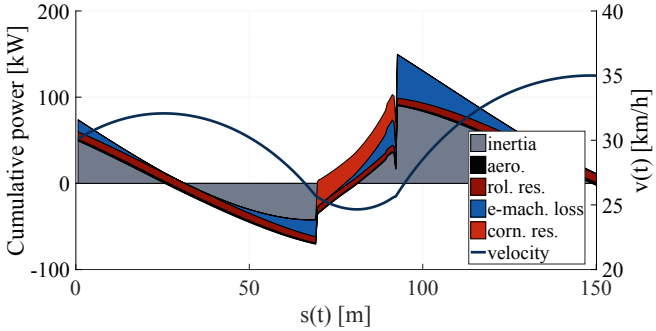

(b) Eco-driving for for general trajectories.

Fig. 6. Velocity and energy losses for a cornering scenario with $R = 14[m]$.

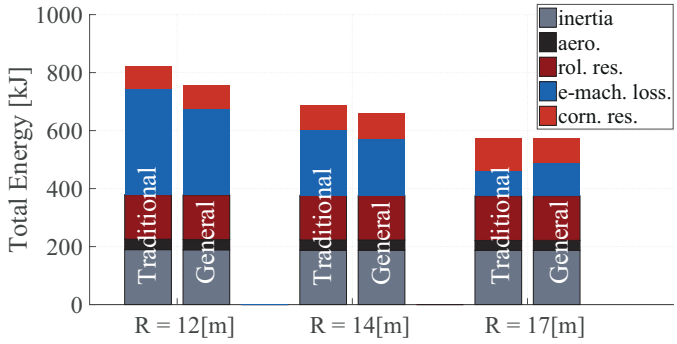

Fig. 7. Cumulative energy consumption for different scenarios and eco-driving strategies.

5. CONCLUSIONS

A model that approximates cornering forces into the longitudinal axis of the vehicle has been proposed in this paper. The simplicity of this model relies on the geometry of the vehicle and the road, which makes it easy to use for a broad spectrum of cases without the necessity of identification of specific tire parameters. Based on this model, we have proposed a general eco-driving optimal control problem formulation that can be used for both straight and curved trajectories. Moreover, it can be used for front wheel drive and rear wheel drive configurations of the vehicle. The advantages of the proposed OCP have been analysed on a case study, where the use of a high-fidelity model have allowed not only to validate the proposed model and OCP formulation, but also to show the improvements of this approach with respect to traditional approaches found in current literature. The results have shown that the use of the general OCP formulation proposed in this paper yields to an improvement energy savings for cornering maneuvers in trajectories with large curvatures, which are approximately up to 8% larger than traditional eco-driving strategies.

REFERENCES

AccessScience Editors (2014). Electric vehicles and range anxiety. doi:10.1036/1097-8542.BR1031141.

Beckers, C., Besselink, I., and Nijmeijer, H. (2020). Assessing the impact of cornering losses on the energy consumption of electric city buses (in press). *Transp. Res. Part D Transp. Environ.*

Bingham, C., Walsh, C., and Carroll, S. (2012). Impact of driving characteristics on electric vehicle energy consumption and range. *IET Intelligent Transport Systems.*

Boyd, S.P. and Vandenberghe, L. (2004). *Convex optimization.* Cambridge University Press.

Edrén, J., Jonasson, M., Jerrelind, J., Stensson Trigell, A., and Drugge, L. (2019). Energy efficient cornering using over-actuation. *Mechatronics.*

Flores, J., Padilla, G., and Donkers, M. (2019). A shrinking horizon approach to eco-driving for electric city buses: Implementation and experimental results. In *IFAC-PapersOnLine*, IFAC Symposium on Advances in Automotive Control.

Grauers, A., Sarasini, S., and Karlström, M. (2013). Why electromobility and what is it? In *Systems Perspectives on Electromobility.*

Han, J., Sciarretta, A., Ojeda, L.L., De Nunzio, G., and Thibault, L. (2018). Safe- and eco-driving control for connected and automated electric vehicles using analytical state-constrained optimal solution. In *IEEE Trans on Intelligent Vehicles.*

Henriksson, M., Flardh, O., and Martensson, J. (2017). Optimal speed trajectories under variations in the driving corridor. In *IFAC World Congress.*

Ikezawa, Y., Fujimoto, H., Kawano, D., Goto, Y., Takeda, Y., and Sato, K. (2017). Range extension autonomous driving for electric vehicle based on optimal vehicle velocity profile in consideration of cornering. *IEEE Trans on Industry Applications.*

Khalik, Z., Padilla, G.P., Romijn, T.C.J., and Donkers, M.C.F. (2018). Vehicle energy management with eco-driving: A sequential quadratic programming approach with dual decomposition. In *American Control Conference.*

Kong, J., Pfeiffer, M., Schildbach, G., and Borrelli, F. (2015). Kinematic and dynamic vehicle models for autonomous driving control design. In *IEEE Intelligent Vehicles Symposium.*

Maamria, D., Gillet, K., Colin, G., Chamaillard, Y., and Nouillant, C. (2017). Optimal eco-driving for conventional vehicles: Simulation and experiment. In *IFAC World Congress, 2017.*

Nunzio, G.D., Wit, C.C.d., Moulin, P., and Domenico, D.D. (2013). Eco-driving in urban traffic networks using traffic signal information. In *Conference on Decision and Control.*

Padilla, G.P., Donkers, M.C.F., and Weiland, S. (2018). A Global Optimal Solution to the Eco-Driving Problem. *IEEE Control Systems Letters.*

Petit, N. and Sciarretta, A. (2011). Optimal drive of electric vehicles using an inversion-based trajectory generation approach. In *IFAC World Congress.*

Polterauer, P., Incremona, G.P., Colancri, P., and Re, L.d. (2019). A switching nonlinear MPC approach for ecodriving. In *American Control Conference.*

Sciarretta, A., Nunzio, G.D., and Ojeda, L.L. (2015). Optimal ecodriving control: Energy-efficient driving of road vehicles as an optimal control problem. *IEEE Control Systems.*